

# COMPUTATIONAL STUDY OF FREE AIR-BREATHING PEM FUEL CELL: SINGLE CELL AND STACK

Agus Pulung Sasmito<sup>1,2,4,5\*</sup>, Erik Birgersson<sup>1,2</sup>, Kah Wai Lum<sup>3</sup>, and Arun Mujumdar<sup>1,4</sup>

<sup>1</sup>Minerals Metals Materials Technology Center (M3TC), National University of Singapore, Singapore, Tel: 971-2-810-9320, e-mail: ap.sasmito@gmail.com

<sup>2</sup>Department of Chemical and Bio-Molecular Engineering, National University of Singapore, Singapore

<sup>3</sup>Institute of High Performance Computing, A\*Star Singapore, Singapore

<sup>4</sup>Department of Mechanical Engineering, National University of Singapore, Singapore

<sup>5</sup>Mechanical Engineering, Masdar Institute of Science and Technology, Abu Dhabi, United Arab Emirates

Received Date: July 4, 2012

## Abstract

The operation of proton exchange membrane (PEM) fuel cell for single cells and stacks with free air-breathing open-cathode manifold requires careful thermal, water and gas management for optimal performance. Here, the cathode channel design and orientation of the cell/stack in the gravitational field are essential due to presence of buoyancy-driven flow. To study the impact of these effects, a three-dimensional two-phase flow model accounting for conservation equations of mass, momentum, species and energy are solved in ambient and cell/stack with additional conservation of charge, agglomerate catalyst layer sub-model and a phenomenological membrane model is considered inside the cell/stack. Three computational units are selected for the cathode flow field design based on the fuel cell length for a single cell: (a) 2.5 cm; (b) 5 cm; and (c) 10 cm. The fourth case (d) considers a stack comprising of twelve cells. Furthermore, the orientation of the fuel cell/stack is studied for the case of horizontal, vertical and a 45° alignment.

Results show that there is a strong correlation between cathode channel design, alignment, thermal management and the cell/stack performance. For the shortest cell (case a), sufficient oxygen can reach the catalyst layer on the cathode side. The longer the cell to height ratio becomes, the higher the degree of oxygen starvation. For the stack (case d), the temperature needs to be carefully monitored and adjusted to the operating conditions of the stack to avoid overheating.

**Keywords:** Buoyancy, Free-air-breathing, Natural convection, PEM fuel cell, Stack

## Introduction

The design of a proton exchange membrane (PEM) fuel cell stack with an open-cathode manifold requires careful consideration of the air flow at the cathodes. The air flow can be provided by a fan (forced convection) or by a passive mechanism such as buoyancy (natural convection). The former will require power for the fan, which has to be supplied by the fuel cell. This parasitic loss can be avoided by employing natural convection, which arises due to density gradients in the air as oxygen is depleted in the cathode, and due to the fuel cell generally being warmer than the surrounding. The main advantages of

operating the fuel cell with natural convection are that the parasitic losses can be reduced and the stack design simplified. However, care has to be taken so as to provide sufficient air to the cathode and to ensure sufficient cooling of the stack. It is relatively easy to control the flow rate with a fan, but this is not the case for natural convection. The operation of a fuel cell stack with natural convection on the cathode side depends on the coupling between heat, mass and momentum transfer both inside and outside the fuel cell stack, which makes it more difficult to control the flow rates for the cathode side.

To date, several experimental [1-5] as well as numerical [6-26] study on the free air-breathing PEM fuel cell have been reported in the literature. Li et al. [6] studied free-convection heat and mass transfer in PEM fuel cell based on non-dimensional analysis. Mennola et al. [7] developed a two-dimensional isothermal, cathode-side model to identify the limiting processes of mass transport due to free-convection. Schimtz et al. [8] developed a 2D, isothermal, steady state model; they investigated three different cathode opening ratios with regard to the cell performance. Wang et al. [9-12] simulated 3D non-isothermal PEM fuel cell with natural convection including its immediate ambient. They also validated the model with experimental data; however, their prediction on temperature increase about 3°C seems to low for natural convection flows. Tabe et al. [13] showed with 3D modeling and experimental data that the mass transport limitation due to oxygen depletion depends strongly on the cathode channel design. Lister et al. [14] simulated micro-structured PEM fuel cell with natural convection where the ambient is also resolved in the model; the model considers two-dimensional, non-isothermal and steady-state condition. Hwang et al. [15] developed a three-dimensional cathode model of a free-breathing PEM fuel cell to investigate mass transport limitations. O'Hayre et al. [16] developed and validated a one-dimensional, non-isothermal engineering model for a planar air-breathing PEM fuel cell.

Rajani and Kolar [17] derived a two-dimensional planar air-breathing model with ambient included in the model; three different fuel cell lengths and ambient conditions were simulated. It was shown that mass transport limitation in the limiting current density region can be reduced by shortening the fuel cell channel in an air-breathing PEM fuel cell Zhang and Pitchumani [18] also simulated two-dimensional non-isothermal air-breathing PEM fuel cell model for a single cell [19] and a stack of two cells [20]. Both gravitational orientation and fuel cell length were included in the model. Matamoros and Bruggemann [21] investigated mass transport limitations and effect of fuel cell length on cell performance with a three-dimensional model of a free-breathing PEM fuel cell. Paquin and Frechette [22] analyzed water management including cathode flooding and membrane dry-out in air breathing PEM fuel cell with a one-dimensional model. Xing et al. [23] optimized the geometry of air-breathing PEM fuel cell with sequential programming method. Al-Baghdadi [24] developed a three-dimensional non-isothermal two-phase model; performance of air-breathing and air-flow channel PEM fuel cell was compared. Kumar and Kolar [25,26] developed a three-dimensional non-isothermal model for air-breathing PEM fuel cell; various cathode channel design and operating parameters were investigated. None of these studies, however, examined three-dimensional free air-breathing PEM fuel cell stack comprise of more than two cells which include interaction between stack and its immediate ambient. In previous work, we have developed a forced-convection open-cathode PEM fuel cell stack model [27,28,29] where the fan and ambient are included in the model, which allows interaction between the stack, the surrounding and the fan. In addition, we have also introduced an innovative flow reversal concept to improve gas and thermal management in PEM fuel cell stack [30]

To extend the work on the PEM fuel cell stack modeling, the aim of the work presented here is threefold: (i) to develop a coupled three-dimensional mathematical model for free

air-breathing PEM fuel cell for both single cell and stack; (ii) to elucidate the effect of fuel cell length and its orientation with regard to the thermal, water and gas management; and (iii) to evaluate ability of natural convection cooling for thermal management in PEM fuel cell comprising large number of cells.

## Model Development

A three-dimensional computational model comprises of PEM fuel cell and its immediate ambient is considered, as illustrated in Figure 1. The PEM fuel cell model consist of a membrane sandwiched by two catalyst layers (cl), two gas diffusion layers (gdl), two flow channels and two current collectors. The flow channels in anode and cathode comprise parallel channels operating in co-flow mode. Symmetry is invoked to the left and right ( $x$ -direction) to reduce computational cost. We assume that in the two-phase flow, the dominating driving force of liquid transport inside the gas diffusion layer and catalyst layer is capillarity. In the flow fields, we consider mist flow approximation.

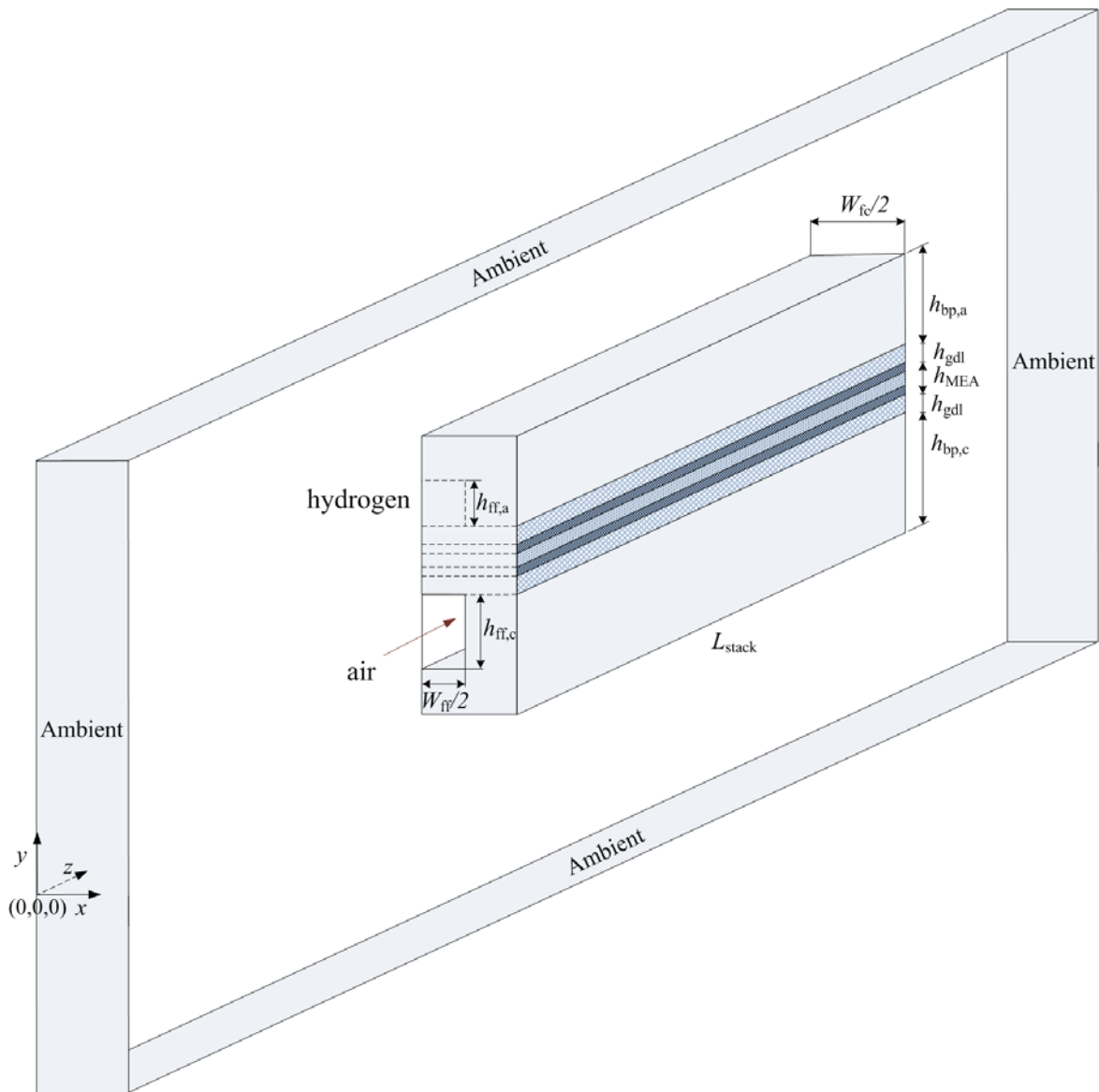


Figure 1. Schematic of computational domain of free air-breathing PEM fuel cell

### Governing Equations

The mathematical formulation is based on earlier work [27-33]: conservation equations of two-phase mass, momentum, species and energy are solved in PEM fuel cell and ambient with additional conservation equations of charge coupled with applicable electrochemistry and a phenomenological membrane model are solved in the PEM fuel cell, expressed as:

$$\tilde{N} \times (r^{(g)} \mathbf{u}^{(g)}) = S_{\text{mass}} - n_{\text{H}_2\text{O}} \quad (1)$$

$$\tilde{N} \times (sr^{(l)} \mathbf{u}^{(l)}) = \tilde{N} \times (D^{(o)} \tilde{N} s) + n_{\text{H}_2\text{O}} \quad (2)$$

$$\tilde{N} \times (r^{(g)} \mathbf{u}^{(g)} \mathbf{u}^{(g)}) = - \tilde{N} p^{(g)} + \tilde{N} \times \left( \frac{\partial}{\partial t} m^{(g)} \mathbf{u}^{(g)} \right) + (\tilde{N} \mathbf{u}^{(g)})^T \frac{\partial}{\partial t} \left( \frac{2}{3} m^{(g)} (\tilde{N} \times \mathbf{u}^{(g)}) \right) + \mathbf{S}_{\text{mom}} \quad (3)$$

$$\tilde{N} \times (r^{(g)} c_p^{(g)} \mathbf{u}^{(g)} T) = \tilde{N} \times (k_{\text{eff}} \tilde{N} T) + S_{\text{temp}} \quad (4)$$

$$\tilde{N} \times (r^{(g)} \mathbf{u}^{(g)} w_i^{(g)}) = \tilde{N} \times (r^{(g)} D_{i,\text{eff}}^{(g)} \tilde{N} w_i^{(g)}) + S_i \quad (i = \text{H}_2, \text{O}_2, \text{H}_2\text{O}, \text{N}_2) \quad (5)$$

$$\tilde{N} \times \left( \frac{\partial}{\partial t} \frac{M_{\text{H}_2\text{O}}}{F} i^{(m)} \right) - \tilde{N} \times \left( \frac{\partial}{\partial t} \frac{r^{(m)}}{M^{(m)}} M_{\text{H}_2\text{O}} D_{\text{H}_2\text{O},\text{eff}}^{(m)} \tilde{N} i \right) = 0 \quad (6)$$

$$\tilde{N} \times (s_{\text{eff}}^{(m)} \tilde{N} f^{(m)}) = - S_{\text{pot}} \quad (7)$$

$$\tilde{N} \times (s_{\text{eff}}^{(s)} \tilde{N} f^{(s)}) = S_{\text{pot}} \quad (8)$$

The source terms in Equations. 1-8 are given by

$$S_{\text{mass}} = \begin{cases} - \frac{M_{\text{O}_2}}{4F} J_c + \frac{M_{\text{H}_2\text{O}}}{2F} J_c - \tilde{N} \times \mathbf{n}_{\text{H}_2\text{O}}^{(m)} & \text{(cathode cl)} \\ - \frac{M_{\text{H}_2}}{2F} J_a - \tilde{N} \times \mathbf{n}_{\text{H}_2\text{O}}^{(m)} & \text{(anode cl)} \\ 0 & \text{(elsewhere)} \end{cases} \quad (9)$$

$$S_{\text{mom}} = \begin{cases} - \frac{m^{(g)}}{k} \mathbf{u}^{(g)} + r^{(g)} \mathbf{g} & \text{(gdl, cl)} \\ r^{(g)} \mathbf{g} & \text{(elsewhere)} \end{cases} \quad (10)$$

$$S_i = \begin{cases} - \frac{M_{\text{O}_2}}{4F} J_c & \text{(O}_2, \text{ cathode cl)} \\ + \frac{M_{\text{H}_2\text{O}}}{2F} J_c - \tilde{N} \times \mathbf{n}_{\text{H}_2\text{O},\text{eff}}^{(m)} - n_{\text{H}_2\text{O}} & \text{(H}_2\text{O, cathode cl)} \\ - \tilde{N} \times \mathbf{n}_{\text{H}_2\text{O},\text{eff}}^{(m)} - n_{\text{H}_2\text{O}} & \text{(H}_2\text{O, anode cl)} \\ - n_{\text{H}_2\text{O}} & \text{(H}_2\text{O, gdl)} \\ - \frac{M_{\text{H}_2}}{2F} J_a & \text{(H}_2, \text{ anode cl)} \\ 0 & \text{(elsewhere)} \end{cases} \quad (11)$$

$$S_{\text{pot}} = \begin{cases} - J_c & \text{(cathode cl)} \\ J_a & \text{(anode cl)} \\ 0 & \text{(elsewhere)} \end{cases} \quad (12)$$

$$S_{temp} = \begin{matrix} J_c \left( \frac{E_{rev}}{T} + h_c \left( \frac{1}{T} + s_{eff}^{(m)} (\tilde{N}f^{(m)})^2 + s_{eff}^{(s)} (\tilde{N}f^{(s)})^2 + n_{H_2O} H_{vap} \right) \right) & \text{(cathode cl)} \\ J_a h_a + s_{eff}^{(m)} (\tilde{N}f^{(m)})^2 + s_{eff}^{(s)} (\tilde{N}f^{(s)})^2 + n_{H_2O} H_{vap} & \text{(anode cl)} \\ s_{eff}^{(m)} (\tilde{N}f^{(m)})^2 & \text{(m)} \\ s_{eff}^{(s)} (\tilde{N}f^{(s)})^2 + n_{H_2O} H_{vap} & \text{(gdl)} \\ s_{eff}^{(s)} (\tilde{N}f^{(s)})^2 & \text{(ff, sp)} \end{matrix} \quad (13)$$

An agglomerate model is implemented to account for mass transfer inside the cathode catalyst layer. Here, we assume the agglomerate nucleus to be spherical in shape, which in turn is covered by a thin film of ionomer and water. For the anode, a conventional expression based on the Butler-Volmer equation is employed as the overpotential is significantly lower than at the cathode.

$$J_a = j_a^{ref} (1 - s) \frac{C_{H_2}^{(g)}}{C_{H_2,ref}^{(g)}} \exp \left( \frac{a_a^{ox} F}{RT} h_a \right) \exp \left( \frac{a_c^{ox} F}{RT} h_a \right) \quad (14)$$

$$J_c = j_c^{ref} \frac{C_{O_2}^{(g)}}{C_{O_2,ref}^{(g)}} \exp \left( \frac{a_a^{rd} F}{RT} h_c \right) + \exp \left( \frac{a_c^{rd} F}{RT} h_c \right) \left( 1 - g_{cl} \right) \left( 1 - \frac{g^{(p)}}{g^{(agg)}} \frac{RT}{H_{O_2}^{(p)}} x_1 \frac{1}{1 + x_2 + x_3} \right) \quad (15)$$

For the sake of brevity, more detailed discussion on the mathematical derivation, constitutive relations, phenomenological membrane model, electrochemistry and agglomerate model can be found in earlier publications [27-33].

### Boundary Conditions

The operating parameters are prescribed from the boundary conditions:

- At the anode inlet: we specify inlet velocity, inlet temperature, and species mass fraction of hydrogen and water vapour represents inlet humidification.

$$u_a = u_a^{in}, T = T^{in}, w_{H_2}^{(g)} = w_{H_2}^{in}, w_{H_2O}^{(g)} = w_{H_2O,a}^{in}, s = 0 \quad (16)$$

- At the anode outlet: we specify pressure and stream-wise gradient of pressure, species and liquid saturation is set to zero; the outlet velocity is not known a priori but needs to be iterated from the neighbouring computational cells.

$$p = p^{ref}, \tilde{N}T = \tilde{N}w_i^{(g)} = \tilde{N}s = 0 \quad (17)$$

- At the ambient: we specify ambient pressure, ambient temperature, and species mass fraction of oxygen and water vapour from ambient humidity condition.

$$p^{(g)} = p^{amb}, T = T^{amb}, w_{O_2}^{(g)} = w_{O_2}^{amb}, w_{H_2O}^{(g)} = w_{H_2O}^{amb}, s = 0 \quad (18)$$

- At walls: we set no slip condition for velocity and zero diffusive flux for other variables.

$$\mathbf{u} = \mathbf{0}, \tilde{N}w_i^{(g)} = \tilde{N}T = \tilde{N}s = \tilde{N}f = 0 \quad (19)$$

- At anode terminal: we specify zero voltage

$$f^{(s)} = 0 \quad (20)$$

- At cathode terminal: we set constant cell/stack voltage.

$$f^{(s)} = E_{\text{cell/stack}} \quad (21)$$

## Numerical Methodology

The governing equations are implemented in the commercial computational fluid dynamics (CFD) software Fluent and its fuel cell module, and further customized with user-defined functions (UDF). The latter allows changes to default settings as well as modifications of the governing equations. In our case, the main parts that we implement with the UDF functionality are: heat generation in the active layers related to the reversible cell potential instead of the open circuit; adaption of the membrane model to a Gore-membrane, implementation of agglomerate catalyst layer model, boundary condition setting and modify the source term for interphase mass transfer.

**Table 1. Base-Case and Geometrical Parameters**

$h_{\text{cc,ff,c}}$	$(0.5, 3) \times 10^{-3}$ m
$h_{\text{ff,a, gdl, cl,m}}$	$(0.5, 0.3, 0.01, 0.05) \times 10^{-3}$ m
$L$	$(2.5, 5, 10) \times 10^{-2}$ m
$p_{\text{amb}}$	101325 Pa
$u_{\text{an,in}}$	2 m s <sup>-1</sup>
$T_{\text{amb}}$	25 °C
$RH_{\text{a,amb}}$	100%, 50%

To ensure mesh-independent results, a mesh-independence study was carried out, with the computational domains created and meshed in the commercial pre-processor software GAMBIT. The various mesh sizes were: around  $1 \times 10^5$ ,  $3 \times 10^5$  and  $6 \times 10^5$  elements for case with fuel cell length of 2.5 cm (case a);  $2 \times 10^5$ ,  $6 \times 10^5$  and  $1.2 \times 10^6$  elements for fuel cell length of 5 cm (case b);  $4 \times 10^5$ ,  $8 \times 10^5$  and  $1.8 \times 10^6$  elements for fuel cell length 10 cm (case c);  $8 \times 10^5$ ,  $1.6 \times 10^6$  and  $3.2 \times 10^6$  elements for stack with 12 cells (case d). For all cases, the two finer meshes produced similar result (deviation less than 1.5 %) while the coarsest gives rise to a difference in the polarization curve of up to 10%, especially so at high current densities. For our purposes, the mesh with  $3 \times 10^5$  elements for case a,  $6 \times 10^5$  elements for case b,  $8 \times 10^5$  elements for case c, and  $1.6 \times 10^6$  for case d were found sufficiently accurate.

A SIMPLE method is chosen for the pressure velocity coupling with body-force-weighted discretization for the pressure equation. Since the model solves for highly coupled non-linear equations, the under-relaxation factors were reduced to 0.75 for the first one thousand iterations and then increased to 1. On average, case a, b and c required around  $1 \times 10^4$  iterations, and case d requires around  $1.5 \times 10^4$  iterations, with convergence criteria for all the relative residuals of  $10^{-6}$ . It took around eighteen and twenty-four hours for case a, b, c and d on a workstation with a quad core processor (2.88GHz) and 8 GB RAM.

## Results and Discussion

Simulations were carried out for typical conditions found in a free air-breathing PEM fuel cell; the geometry and operating parameters are summarized in Table 1; while the remaining physical parameters can be found in [27-33]. The fuel cell model was validated against polarization curves, iR corrected curves and local current density distribution in

previous work [31-33]. In the following, key parameters related to thermal, water and gas management as well as the stack performance will be studied for three different fuel cell length and three different gravitational orientation, after which the effect large number of cells inside the stack is examined with regard to the thermal management and its overall performance.

### Cathode Channel Designs

Starting with the performance of the three different cathode channel lengths, we find that case c, i.e. the shortest cathode channel ( $L = 2.5$  cm), exhibits the best performance as shown in Figure 2. Furthermore, as can be inferred from Figure 2, the longer the channel the lower the performance. We note that the limiting current for the shortest length goes up to more than  $4000 \text{ A m}^{-2}$ , and reduces to  $2000$  and  $1000 \text{ A m}^{-2}$  as the length increased twice and four times, respectively.

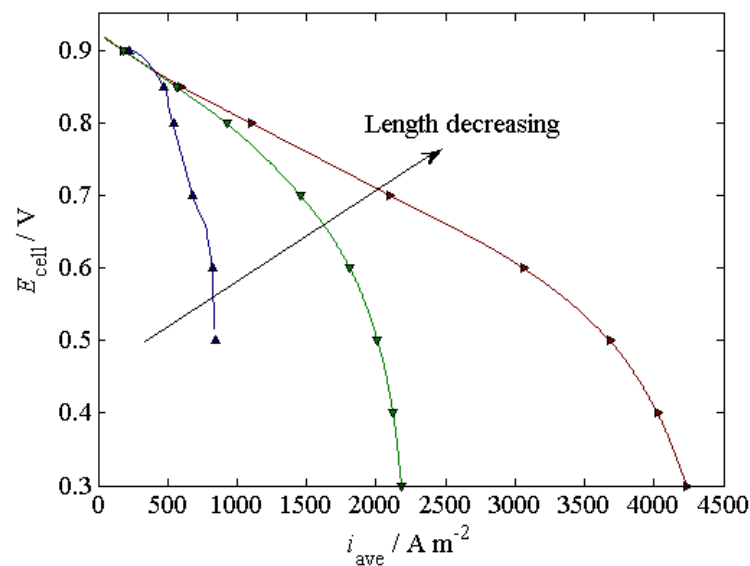


Figure 2. Polarization curves for free air-breathing PEM fuel cell with length of 2.5 cm [▶], 5 cm [▼], and 10 cm [▲]

Before we try to find the answer to this decrease, let us turn our attention towards the current density distribution along the catalyst area. Here, several features are apparent; foremost is that the current density along the fuel cell channel is higher near the two cathode inlets (to the top and bottom), as can be inferred in Figure 3. For the shortest length, the current is seen to be generated quite uniformly with around 10% deviation. As the fuel cell length increases, current generation becomes greatly non-uniform. Closer inspection reveals that current generation reduces up to 75% at the middle area for fuel cell length 5 cm and become worse for fuel cell length 10 cm with almost no current is seen to be generated at the middle area.

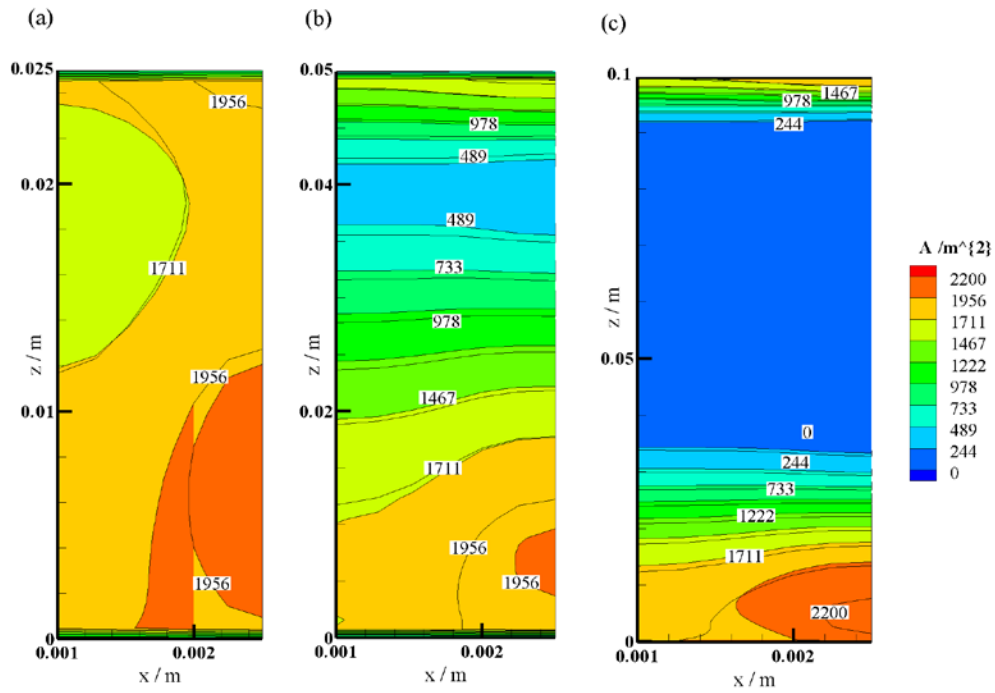


Figure 3. Current density distribution ( $A/m^2$ ) at the cathode catalyst layer for different fuel cell lengths: a) 2.5 cm; b) 5 cm; c) 10 cm

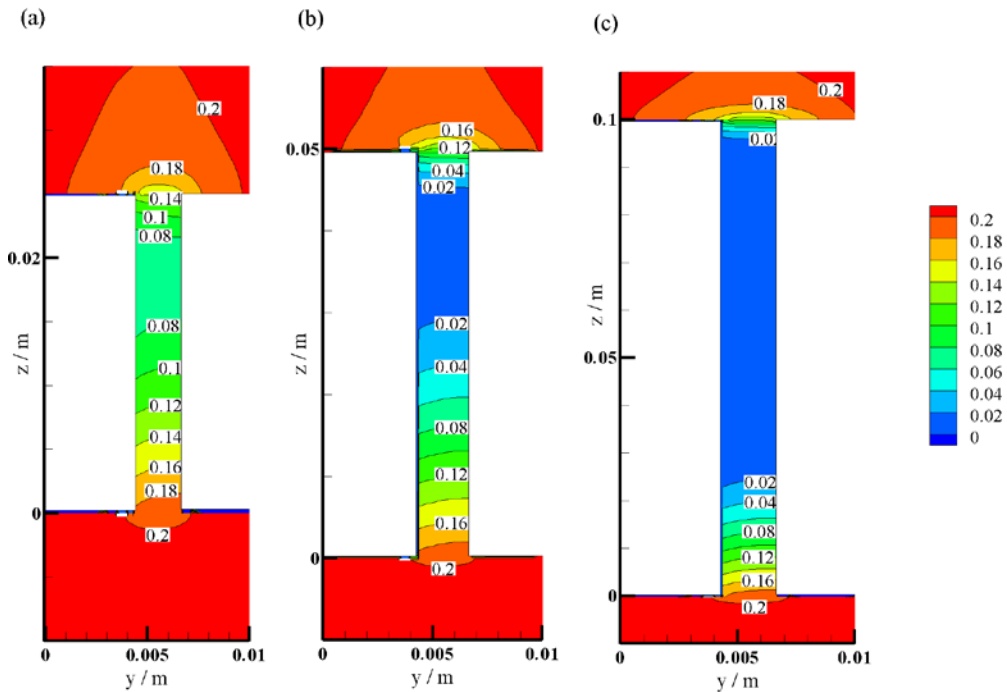


Figure 4. Oxygen mol fraction distribution at the cathode and its immediate ambient for fuel cell lengths of ( a) 2.5 cm, (b) 5 cm and (c) 10 cm

Now, returning to the question about current density depletion in the middle of the channel, we see that the answer is directly coupled to the depletion of the oxygen concentration in the middle of the channel, as can be inferred from Figure 4. Clearly, the convective flow of oxygen driven by natural convection into the cathode channel is not high enough to penetrate deeper into the cathode flow field to produce electricity. This mass transport limitation can be reduced by shortening the cathode flow field, so that the oxygen still can reach to the middle, as can be seen in Figure 4a.

### Orientation and Gravitational Effects

The flow arising from natural convection depends on the coupling between transport of mass, energy and momentum and the variation of the density. The orientation of the fuel cell/stack can therefore be expected to have an impact on the performance. To study if this is the case, let us return to case b and introduce three different orientations: vertical ( $90^\circ$ , base-case); tilted ( $45^\circ$ ); horizontal ( $0^\circ$ ), as shown in Figure 5.

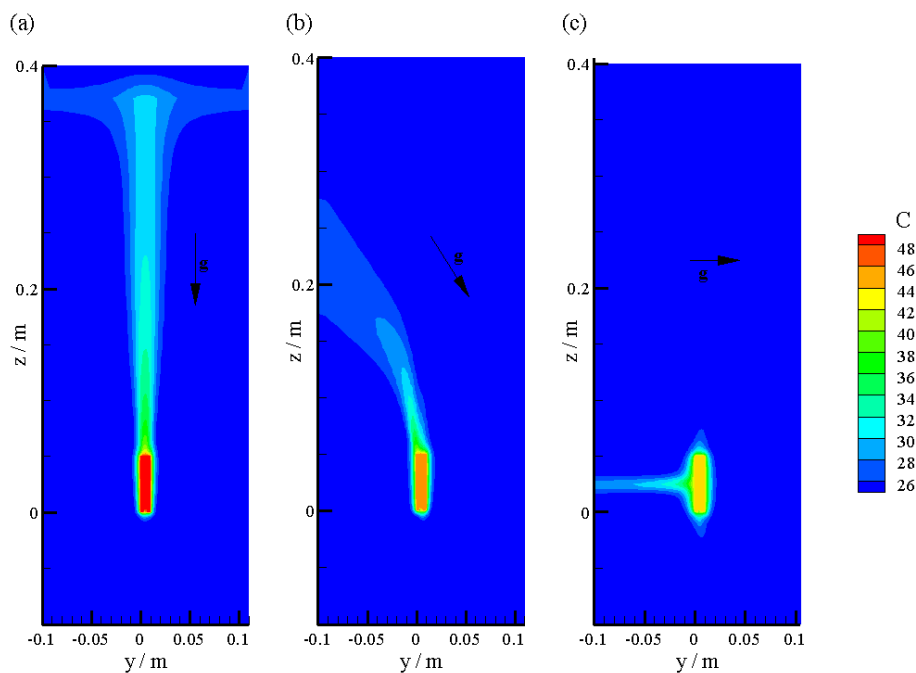


Figure 5. Temperature distribution ( $^\circ\text{C}$ ) for different gravitational orientations: a) vertical ( $90^\circ$ ); b) tilted ( $45^\circ$ ); c) horizontal ( $0^\circ$ )

Before we look into cell performance, let us have a closer look at the temperature distribution, which is one of the driving forces for the density variations and buoyant flow. As shown in Figure 5, the temperature distribution is similar to the thermal plume that Fabian et al. [34] observed experimentally. Focusing on case a, and the immediate vicinity of the cell, as depicted in Figure 6, we find that the average velocity is around  $2 \times 10^{-2} \text{ m s}^{-1}$  at the cathode inlets arising from buoyancy flowing from bottom to the top. For tilted case, a slightly lower velocity is observed flowing at the bottom of the cathode channel with the average velocity of around  $8 \times 10^{-3} \text{ m s}^{-1}$ . In contrast, for the horizontal placement, the inlet velocity is around one order-of-magnitude lower with an average flow velocity of  $3 \times 10^{-3}$ . In addition, the maximum velocity due to natural convection in the surrounding is around  $5 \times 10^{-2} \text{ m s}^{-1}$ , which is similar to the velocities predicted by Lister et al. [14].

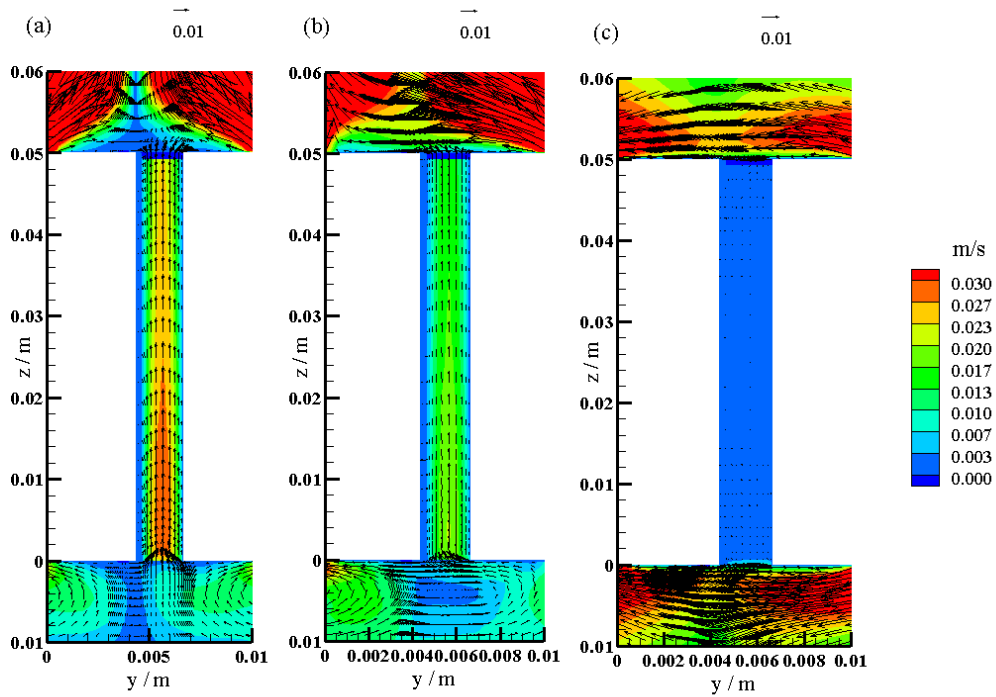


Figure 6. Velocity vector and contour ( $\text{ms}^{-1}$ ) at the cathode and its immediate ambient for different gravitational orientations: a) vertical ( $90^\circ$ ); b) tilted ( $45^\circ$ ); c) horizontal ( $0^\circ$ )

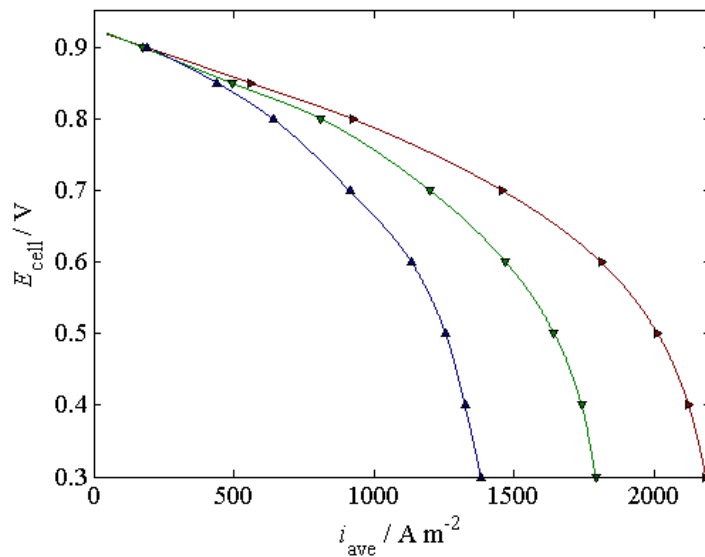


Figure 7. Polarization curves for different gravitational orientations: [►] vertical ( $90^\circ$ ); [▼] tilted ( $45^\circ$ ); and [▲] horizontal ( $0^\circ$ )

In free-breathing fuel cell, the velocity is highly nonlinear as it is functions of buoyancy flow due to temperature gradient, flow channel geometry and orientations as well as mass transfer driving force due to oxygen consumption. Note that in this simulation, the air flow rate is not fixed; instead we prescribe ambient condition, i.e., constant ambient pressure, temperature and mass fraction, to allow for natural convection air flow due to the factors mentioned above. Moreover, the three-dimensional simulation is able to capture the

effect of channel-rib geometry to the incoming air flow and species distribution in the catalyst layer. Closer inspection reveals that rib adds flow resistant to the incoming air to flow channel: small boundary layer is observed at the wall between rib-ambient. In the catalyst layer, the three-dimensionality effect of rib is also seen: oxygen concentration bellow rib area is slightly lower than that bellow channel; this is mirrored by no-uniform current generation and temperature distribution.

The impact of orientation on fuel cell performance is highlighted in Figure 7. The highest performance can be achieved by vertical alignment of the cell, followed by tilted case and finally the horizontal one for the operating conditions considered here. On closer inspection, we note that by changing gravitational orientation, the cell performance can improve by up to ~ 35%; that is by changing cell orientation from horizontal with limiting current of ~ 1300 A m<sup>-2</sup> improves to around 2300 A m<sup>-2</sup> as the cell is arranged vertically.

### Thermal Management: Single Cell and Stack

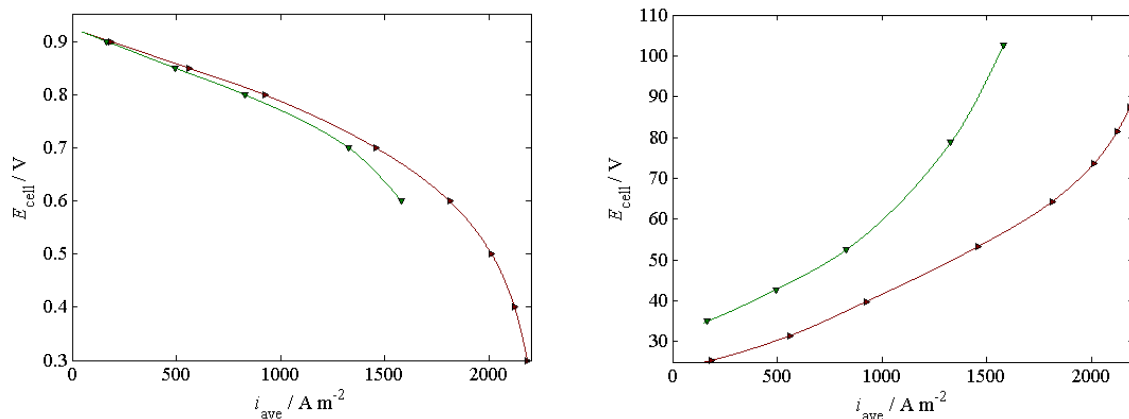


Figure 8. Comparison of (a) polarization curve and (b) average temperature for single cell [►] and stack comprises of 12 cells [▼] with free air-breathing

One key component in control strategies of a fuel cell stack or single cell is thermal management. This is especially important for the former as every cell can generate a significant amount of heat, which needs to be removed from the stack. For the case of a fuel cell single cell or stack operating at natural convection conditions, the removal rate is limited by the natural convection to and from the cell/stack. Generally, this only allows for the operation of small stacks of a few cells. Here, we simulate the thermal envelope for both a single cell and a stack comprising of twelve cells, the results of which are shown in Figure 8.

The temperature increase for the stack is much higher than the single cell as expected. The overall temperature increase for the latter is around 23°C at operating cell voltage of 0.7 V (see Figure 9a), which is in agreement with experimental data from Fabian et al. [34]. For the former, the stack temperature is around 55°C higher than the ambient air (Figure 9b). The higher temperature inside each cell of the stack leads to a lower water content in the membranes and thus an increase in ohmic resistance, which in turn manifests itself in a lower performance. In this case, the overall current density that is generated by the stack is around 20% lower than that of the single cell. As we proceed to higher current densities, the single cell performance can sustain up to more than 2000 A m<sup>-2</sup>; whereas for stack, the performance is only able to generate current density up to ~ 1600 A m<sup>-2</sup>, after which the performance drops to zero as temperature inevitably rise to more than 100°C which

indicates that membrane start to failure. To improve performance of the stack, one needs to carefully design it to maximize the buoyant flow and perhaps introduce additional cooling channels or add fan to forced more air flows to the cathode.

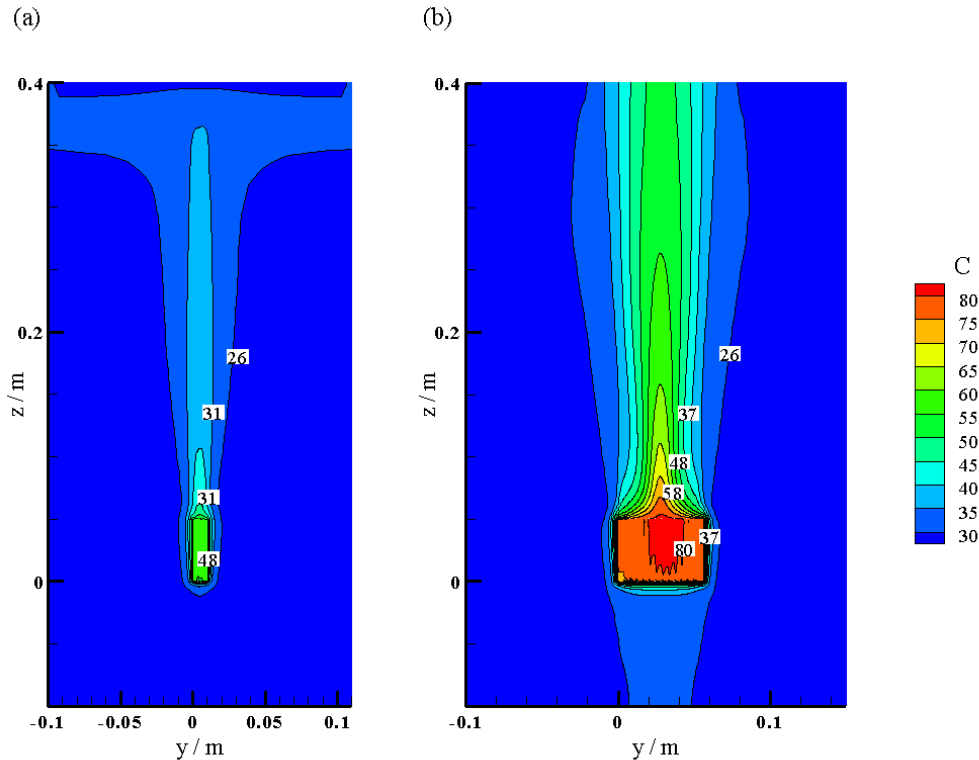


Figure 9. Temperature contours ( $^{\circ}\text{C}$ ) for a) single cell; b) stack comprising 12 cells with its immediate ambient

## Concluding Remarks

A numerical study of a free air-breathing PEM fuel cell was carried out for both a single cell and a stack. It is shown that the cathode flow field design plays an important role in determining the mass transport limitations that arise along the cathode; a short length allows for more oxygen to be transported into the cathode. Furthermore, orientation of the cell/stack with respect to gravity also needs to be considered to ensure adequate airflow; for conditions considered here, a vertical alignment of the cell gave a better performance than tilting the cell at an angle or even positioning it horizontally. Finally, the simulation results indicate that stacks, even when only comprising of a few cells, can heat up significantly relative to the ambient conditions.

## Acknowledgement

The financial support of the National University of Singapore (NUS) and the ASEAN University Network/ South-East Asia Engineering Education Development-Network (AUN/SEED-Net) are gratefully acknowledged.

## References

- [1] S. Hamel, and L.G. Frechette, "Critical importance of humidification of the anode in miniature air-breathing polymer electrolyte membrane fuel cells," *Journal of Power Sources*, Vol. 196, pp. 6242-6248, 2011.
- [2] Z.R. Williamson, D. Kim, D.K. Chun, T. Lee, and C.W. Squibb, "Experimental evaluation of cell temperature effects on miniature air breathing PEM fuel cells," *Applied Thermal Engineering*, 2011, doi: 10.1016/j.applthermaleng. 2011. 06.10.
- [3] C.K. Poh, Z. Tian, N. Bussayajarn, Z. Tang, F. Su, S.H. Lim, Y.P. Feng, D. Chua, and J. Lin, "Performance enhancement of air-breathing proton exchange membrane fuel cell through utilization of an effective self-humidifying platinum-carbon catalyst," *Journal of Power Sources*, Vol. 195, pp. 8044-8051, 2010.
- [4] K.I. Lee, S.W. Lee, M.S. Park, and C.N. Chu, "The development of air-breathing proton exchange membrane fuel cell (PEMFC) with a cylindrical configuration," *International Journal of Hydrogen Energy*, Vol. 35, pp. 11844-11854, 2010.
- [5] N. Bussayajarn, H. Ming, K.K. Hoong, W.Y.M. Stephen, and C.S. Hwa, "Planar air breathing PEMFC with self-humidifying MEA and open cathode geometry design for portable applications," *International Journal of Hydrogen Energy*, Vol. 34, pp. 7761-7767, 2009.
- [6] P.W. Li, T. Zhang, Q.M. Wang, L. Schaefer, and M.K. Chyu, "The performance of PEM fuel cells fed with oxygen through the free-convection mode," *Journal of Power Sources*, Vol. 114, pp. 63-69, 2003.
- [7] T. Mennola, M. Noponen, M. Aronniemi, T. Hottinen, M. Mikkola, O. Himanen, and P. Lund, "Mass transport in the cathode of a free-breathing polymer electrolyte membrane fuel cell," *Journal of Applied Electrochemistry*, Vol. 33, pp. 979-987, 2003.
- [8] A. Schmitz, C. Ziegler, J.O. Schumacher, M. Tranitz, E. Fontes, and C. Hebling, "Modelling approach for planar self-breathing PEMFC and comparison with experimental results," *Fuel Cells*, Vol. 4, pp. 358-364, 2004.
- [9] Y. Wang, Y.J. Sohn, W.Y. Lee, J. Ke, and C.S. Kim, "Three-dimensional modeling and experimental investigation for an air-breathing polymer electrolyte membrane fuel cell PEMFC," *Journal of Power Sources*, Vol. 145, pp. 563-571, 2005.
- [10] Y. Wang, T.H. Yang, W.Y. Lee, J. Ke, and C.S. Kim, "Three-dimensional analysis for effect of channel configuration on the performance of a small air-breathing proton exchange membrane fuel cell (PEMFC)," *Journal of Power Sources*, Vol. 145, pp. 572-581, 2005.
- [11] Y. Wang, J. Ke, W.Y. Lee, T.H. Yang, and C.S. Kim, "Effects of cathode channel configurations on the performance of an air-breathing PEMFC," *International Journal of Hydrogen Energy*, Vol. 30, pp. 1351-1361, 2005.
- [12] Y. Wang, and M. Ouyang, "Three-dimensional heat and mass transfer analysis in an air-breathing proton exchange membrane fuel cell," *Journal of Power Sources*, Vol. 164, pp. 721-729, 2007.
- [13] Y. Tabe, S.K. Park, K. Kikuta, T. Chikahisa, and Y. Hishinuma, "Effect of cathode separator structure on performance characteristics of free-breathing PEMFCs," *Journal of Power Sources*, Vol. 162, pp. 58-65, 2006.
- [14] S. Lister, J.G. Pharoah, G. McLean, and N. Djilali, "Computational analysis of heat and mass transfer in a micro-structured PEMFC cathode," *Journal of Power Sources*, Vol. 156, pp. 334-344, 2005.
- [15] J.J. Hwang, "Species-electrochemical modeling of an air-breathing cathode of a planar fuel cell," *Journal of the Electrochemical Society*, Vol. 153, pp. A1584-A1590, 2006.

- [16] J.J. Hwang, S.D. Wu, R.G. Pen, P.Y. Chen, and C.H. Chao, "Mass/electron co- transports in an air-breathing cathode of a PEM fuel cell," *Journal of Power Sources*, Vol. 160, pp. 18-26, 2006.
- [17] R. O'Hayre, T. Fabian, S. Litster, F.B. Prinz, and J.G. Santiago, "Engineering model of a passive planar air breathing fuel cell cathode," *Journal of Power Sources*, Vol. 167, pp. 118-129, 2006.
- [18] B.P.M. Rajani, and A.K. Kolar, "A model for a vertical planar air breathing PEM fuel cell," *Journal of Power Sources*, Vol. 164, pp. 210-221, 2007.
- [19] Y. Zhang, and R. Pitchumani, "Numerical studies on an air-breathing proton exchange membrane PEM fuel cell," *International Journal of Heat and Mass Transfer*, Vol. 50, pp. 4698-4712, 2007.
- [20] Y. Zhang, A. Mawardi, and R. Pitchumani, "Numerical studies on an air-breathing proton exchange membrane PEM fuel cell stack," *Journal of Power Sources*, Vol. 173, pp. 264-276, 2007.
- [21] L. Matamoros, and D. Bruggemann, "Concentration and ohmic losses in free-breathing PEMFC," *Journal of Power Sources*, Vol. 173, pp. 367-374, 2007.
- [22] M. Paquin, and L. Frechete, "Polarization study of a PEMFC with four reference electrodes at hydrogen starvation conditions," *Journal of Power Sources*, Vol. 180, pp. 440-451, 2008.
- [23] X.Q. Xing, K.W. Lum, H.J. Poh, and Y.L. Wu, "Geometry optimization for proton-exchange membrane fuel cells with sequential quadratic programming method," *Journal of Power Sources*, Vol. 186, pp. 10-21, 2009.
- [24] M.A.R.S. Al-Baghdadi, "Performance comparison between airflow-channel and ambient air-breathing PEM fuel cells using three-dimensional computational fluid dynamics models," *Renewable Energy*, Vol. 34, pp. 1812-1824, 2009.
- [25] P.M. Kumar, and A.K. Kolar, "Effect of cathode design on the performance of an air-breathing PEM fuel cell," *International Journal of Hydrogen Energy*, Vol. 35, pp. 671-681, 2010.
- [26] P.M. Kumar, and A.K. Kolar, "Effect of cathode channel dimensions on the performance of an air-breathing PEM fuel cell," *International Journal of Thermal Sciences*, Vol. 49, pp. 844-857, 2010.
- [27] A.P. Sasmito, K.W. Lum, E. Birgersson, and A.S. Mujumdar, "Computational study of forced air-convection in open-cathode polymer electrolyte fuel cell stacks," *Journal of Power Sources*, Vol. 195, pp. 5550-5563, 2010.
- [28] A.P. Sasmito, E. Birgersson, K.W. Lum, and A.S. Mujumdar, "Fan selection and stack design for open-cathode polymer electrolyte fuel cell stacks," *Renewable Energy*, Vol. 37, pp. 325-332, 2012.
- [29] A.P. Sasmito, E. Birgersson, and A.S. Mujumdar, "Numerical evaluation of various thermal management strategies for polymer electrolyte fuel cell stacks," *International Journal of Hydrogen Energy*, Vol. 36, pp. 12991-13007, 2011.
- [30] A.P. Sasmito, and A.S. Mujumdar, "A novel flow reversal concept for improved thermal management in polymer electrolyte fuel cell stacks," *International Journal of Thermal Sciences*, Vol. 54, pp. 242-252, 2012.
- [31] A.P. Sasmito, and A.S. Mujumdar, *Transport Phenomena Models for Polymer Electrolyte Fuel Cell Stacks: Thermal, Water and Gas Management - From Fundamentals to Applications*, Lambert Academic Publishing, Germany, 2011.
- [32] A.P. Sasmito, E. Birgersson, and A.S. Mujumdar, "Numerical investigation of liquid water cooling for a proton exchange membrane fuel cell stack," *Heat Transfer Engineering*, Vol. 32, pp. 151-167, 2011.
- [33] A.P. Sasmito, and A.S. Mujumdar, "Performance evaluation of a polymer electrolyte

- fuel cell with a dead-end anode: A computational fluid dynamic study,” *International Journal of Hydrogen Energy*, Vol. 36, pp. 12991-13007, 2011.
- [34] T. Fabian, J.D. Posner, R. O’Hayre, S.W. Cha, J.K. Eaton, F.B. Prinz, and J.G. Santiago, “The role of ambient conditions on the performance of a planar air-breathing hydrogen PEM fuel cell,” *Journal of power Sources*, Vol. 161, pp. 168-182, 2006.